good account of spectral observations. We will show elsewhere that enough independent broken symmetry molecular orbital calculations can be computed to determine all of the parameters in this spin Hamiltonian as well. Thus the scheme outlined here should enable connections to be made between spin Hamiltonian models and practical calculations for a wide range of localized and delocalized polynuclear transition-metal complexes.

Note Added in Proof. Magnetic susceptibility measurements on the oxidized 3-Fe cluster in *D. gigas* yield $J > 200$ cm^{-1}, in qualitative agreement with the present results.[26]

Acknowledgment. We thank Eckard Münck for many useful discussions and the National Science Foundation for financial support. L.N. thanks C.E.N.G. and the University of Grenoble for their hospitality and J. Gaillard, J. J. Girerd, J. M. Moulis, J. Meyer, J. Jordanov, and B. Lamotte for valuable discussions.

Registry No. Fe, 7439-89-6; S, 7704-34-9.

(24) Guigliaretti, B.; Gayda, J. P.; Bertrand, P.; More, C. *Biochim. Biophys. Acta* **1986**, *871*, 149. Buigliaretti, B.; More, C.; Bertrand, P.; Gayda, J. P. *J. Chem. Phys.* **1986**, *85*, 2774.
(25) Palmer, G. In *Iron-Sulfur Proteins*; Lovenberg, W., Ed.; Academic Press: New York, 1973; Vol. 2, pp 285-325. Kimura, T.; Tasaki, A.; Watari, H. *J. Biol. Chem.* **1970**, *245*, 4450. Molski, C.; Moss, T. H.; Orme-Johnson, W. H.; Tsibris, J. C. M. *Biochim. Biophys. Acta* **1970**, *214*, 548.
(26) Day, E. P.; Peterson, J.; Bonvoisin, J. J.; Moura, I.; Moura, J. J. G. *J. Biol. Chem.*, in press.

Ultraviolet Resonance Raman Excitation Profiles of Tyrosine: Dependence of Raman Cross Sections on Excited-State Intermediates

Michael Ludwig and Sanford A. Asher*

Contribution from the University of Pittsburgh, Department of Chemistry, Pittsburgh, Pennsylvania 15260. *Received March 20, 1987*

Abstract: Ultraviolet resonance Raman (UVRR) excitation profiles have been measured for tyrosine with excitation between 217 and 240 nm. Resonance excitation enhances Raman scattering from vibrational modes that distort the ground-state configuration toward the configuration of the excited state. The excitation profiles of tyrosine, in conjunction with previously presented excitation profiles of tyrosinate, indicate the sensitivity and selectivity available for excitation of tyrosyl residues in proteins. Parameters are developed for the choice of excitation wavelength for the study of tyrosyl residues in proteins. A model is developed which predicts the effect of increasing the incident laser power on the measured Raman cross sections and excitation profiles. The model specifically includes depletion of ground-state analyte molecules and population of excited-state (spectroscopically silent) intermediates. The effects of optical saturation phenomena on UVRR studies of proteins are discussed.

Ultraviolet resonance Raman spectroscopy (UVRR) is a powerful new technique for physical, biophysical, and analytical studies. This technique offers a means of studying molecular structure and dynamics both in the excited and ground states of molecules.[1-21] In a wide range of biological applications, RR has been used to study proteins and nucleic acids, as well as to probe the mechanism of energy transduction in visual processes,[22,23] and ligand binding to prosthetic groups of heme proteins.[22-26] Recent UVRR studies in this and other laboratories have shown the potential of the technique, but have also demonstrated the experimental difficulties inherent to UVRR.[28,29] While the selective enhancement of individual aromatic amino acids is possible with excitation wavelengths between 220 and 250 nm,[21] a combination of photochemical and saturation effects can make UVRR measurements extremely difficult. The difficulties encountered in the study of monomeric aromatic amino acid solutions can be expected to also arise in studies of proteins.

In this report we examine the UV resonance Raman excitation profiles of aqueous solutions of tyrosine. These excitation profiles, in conjunction with the previously reported excitation profiles of tyrosinate,[21] indicate the selectivity available for UVRR excitation of individual tyrosyl residues in proteins. The excitation profiles also contain information about the excited states of tyrosine, since the degree of enhancement of a given vibrational band is related

(1) Asher, S. A.; Johnson, C. R.; Murtaugh, J. *Rev. Sci. Instrum.* **1983**, *54*, 1657.
(2) Asher, S. A.; Johnson, C. R. *J. Phys. Chem.* **1985**, *89*, 1375.
(3) Jones, J. M.; Johnson, C. R.; Asher, S. A.; Shepherd, R. E. *J. Am. Chem. Soc.* **1985**, *107*, 3772.
(4) Ziegler, L. D.; Hudson, B. S. *J. Chem. Phys.* **1981**, *74*, 982.
(5) Ziegler, L. D.; Hudson, B. S. *J. Chem. Phys.* **1983**, *79*, 1134.
(6) Ziegler, L. D.; Hudson, B. S. *J. Phys. Chem.* **1984**, *88*, 1110.
(7) Ziegler, L. D.; Hudson, B. S. *J. Chem. Phys.* **1983**, *79*, 1197.
(8) Mayne, L. C.; Ziegler, L. D.; Hudson, B. S. *J. Phys. Chem.* **1985**, *89*, 3395.
(9) Ziegler, L. D.; Kelley, P. B.; Hudson, B. S. *J. Chem. Phys.* **1984**, *81*, 6399.
(10) Korenowski, G. M.; Ziegler, L. D.; Albrecht, A. C. *J. Chem. Phys.* **1978**, *68*, 1248.
(11) Jones, C. M.; Naim, T.; Ludwig, M.; Murtaugh, J.; Flaugh, P. F.; Dudik, J. M.; Johnson, C. R.; Asher, S. A. *Trends Anal. Chem.* **1985**, *4*, 75.
(12) Asher, S. A.; Johnson, C. R. *Science* **1984**, *225*, 311.
(13) Johnson, C. R.; Asher, S. A. *Anal. Chem.* **1984**, *56*, 2258.
(14) Foder, S. P. A.; Rava, R. P.; Hays, T. R.; Spiro, T. G. *J. Am. Chem. Soc.* **1985**, *107*, 1520.
(15) (a) Rava, R. P.; Spiro, T. G. *J. Am. Chem. Soc.* **1984**, *106*, 4062. (b) Rava, R. P.; Spiro, T. G. *J. Phys. Chem.* **1985**, *89*, 1856.
(16) Rava, R. P.; Spiro, T. G. *Biochemistry* **1985**, *24*, 1861.
(17) Copeland, R. A.; Dasgupta, S.; Spiro, T. G. *J. Am. Chem. Soc.* **1985**, *107*, 3370.
(18) Johnson, C. R.; Ludwig, M.; O'Donnell, S. E.; Asher, S. A. *J. Am. Chem. Soc.* **1984**, *106*, 5008.
(19) Dudik, J. M.; Johnson, C. R.; Asher, S. A. *J. Phys. Chem.* **1985**, *89*, 3805.
(20) Johnson, C. R.; Asher, S. A. *J. Raman Spectrosc.* **1987**, *18*, 345.
(21) Asher, S. A.; Ludwig, M.; Johnson, C. R. *J. Am. Chem. Soc.* **1986**, *108*, 3186.
(22) Carey, P. R. *Biological Applications of Raman and Resonance Raman Spectroscopies*; Academic Press: New York, 1982.
(23) Tu, A. T. *Raman Spectroscopy in Biology: Principles and Applications*; Wiley: New York, 1982.
(24) Asher, S. A. *Methods Enzymol.* **1981**, *76*, 371.
(25) Spiro, T. G. In *The Porphyrins*; Lever, A. B. P., Graya, H. B., Eds.; Addison-Wesley: Reading, MA, 1983; part II, p 89.
(26) Larkin, P. J.; Asher, S. A., in preparation.
(27) Dudik, J. M.; Johnson, C. R.; Asher, S. A. *J. Chem. Phys.* **1985**, *82*, 1732.
(28) Johnson, C. R.; Ludwig, M.; Asher, S. A. *J. Am. Chem. Soc.* **1986**, *108*, 905.
(29) Jones, C. M.; Asher, S. A., in preparation.

0002-7863/88/1510-1005$01.50/0 © 1988 American Chemical Society

to the differences in electron density and geometry between the ground and excited states,[19,21,27] and the width of the excitation profiles depends on the excited-state lifetime. The effect of pH on the resonance Raman spectrum of tyrosine is discussed, and the excitation profiles of tyrosine are compared to those of tyrosinate. The optical saturation phenomena observed derive from a depletion of the population of ground-state molecules available for Raman scattering. We have successfully modeled this saturation based on the absorption spectrum of tyrosine and the incident laser power. This model provides insight into the mechanism of optical saturation, and predicts the effects of saturation on the observed Raman excitation profiles. The experimental consequences of optical saturation on UV Raman studies of proteins are discussed.

Experimental Section

Tyrosine, obtained from Sigma Chemical Co. (St. Louis, MO), was used as supplied to prepare solutions (1.0 mM) in aqueous phosphate buffer (0.04 M, pH 6.1). The samples contained sodium perchlorate (1.0 M) as an internal intensity standard. The Raman spectra of the solutions were measured in a flowing closed cycle recirculating stream in which the solutions were pumped through a 1.0-mm i.d. Suprasil quartz capillary tube. The scattered light was collected at 90°.

The Raman spectrometer has been described in detail elsewhere.[1,30] The excitation source is a Quanta-Ray DCR-2A Nd-YAG laser operated at 20 Hz and frequency doubled to pump a dye laser. UV light is generated by mixing the frequency doubled dye laser output with the 1.06-μm fundamental of the YAG laser. An ellipsoidal mirror was used to collect the scattered light to avoid chromatic aberrations. The polarization of the scattered light was randomized by a crystalline quartz wedge to avoid intensity artifacts deriving from any polarization efficiency bias of the monochromator (modified Spex Triplemate). The scattered light was detected with a Princeton Applied Research OMA II system which utilizes a Model 1420 blue-enhanced intensified Reticon detector.

The excitation profile data derive from peak area measurements. The intensity ratios were corrected for monochromator and detector efficiencies. The total differential Raman cross sections of tyrosine were calculated from the known cross sections of perchlorate.[27] In order to reduce nonlinear optical processes and the formation of high concentrations of photochemical transient species, which are major impediments for Raman intensity measurements of tyrosine, the laser power density within the sample was minimized during the excitation profile measurements. The power of the beam was attenuated by using neutral density filters.

The 10-mL samples of 1.0 mM tyrosine were irradiated for 15 min using energies of less than 0.05 mJ/pulse at a pulse repetition rate of 20 Hz. The laser beam was defocused at the capillary, with an estimated diameter of 2.0 mm. The net photon flux averaged over 1/e of the Gaussian beam profile, as incident on the 1.0-mm capillary volume containing the sample at 220-nm excitation corresponds to about one photon per nine tyrosine molecules. The maximum sample OD was 9 for a 1-cm path length. Thus, the incident power over the 1-mm sample path length was reasonably uniform. The power flux and energy flux incident on the sample under the described conditions were less than 300 kW/cm^2 and 1 mJ/cm^2 pulse, respectively.

The absorption spectra of the solutions, measured before and after the Raman measurements, demonstrate that no significant photochemical decomposition occurred. Under the conditions used for the excitation profile measurements, the Raman intensities of tyrosine and perchlorate bands increase linearly with increases in incident laser intensity.

The spectra collected with low average incident power levels (less than 0.05 mJ/pulse) were Fourier transformed and the high-frequency noise components were removed to improve the signal-to-noise ratios prior to peak area measurements. Depolarization ratios were measured with 225-nm excitation using a Polacoat analyzer. The depolarization ratios were measured using 40 mW of defocused incident laser radiation.

Results

The absorption spectra of tyrosine (pH 6.1 in phosphate buffer) and tyrosinate (pH 11.5) are shown in Figure 1. Tyrosine exhibits absorption maxima at 222 nm (L_a, ϵ = 9000 M^{-1} cm^{-1}) and 275 nm (L_b, ϵ = 1400 M^{-1} cm^{-1}), while tyrosinate shows maxima at 240 nm (L_a, ϵ = 11 000 M^{-1} cm^{-1}) and 293 nm (L_b, ϵ = 2300 M^{-1} cm^{-1}). These transitions derive from the B_{1u} (L_a) and B_{2u} (L_b)

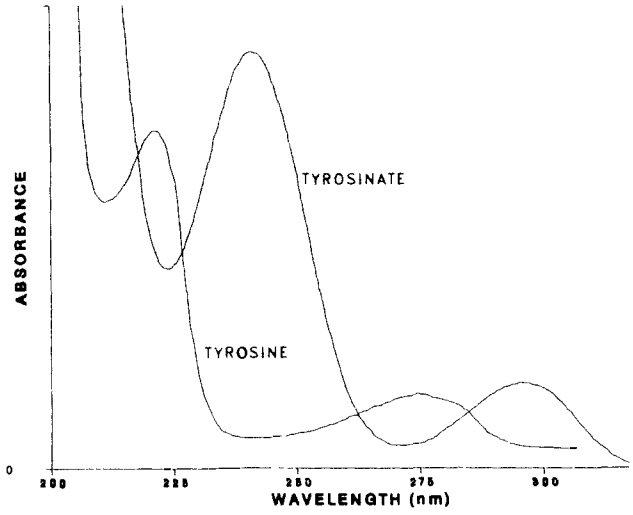

Figure 1. Absorption spectra of aqueous solutions of tyrosine (pH 6.0 in phosphate buffer, L_a max 222 nm, ϵ 9000 M^{-1} cm^{-1}; L_b max 275 nm, ϵ 1400 M^{-1} cm^{-1}) and tyrosinate (pH 11.5, L_a max 240 nm, ϵ 11 000 M^{-1} cm^{-1}; L_b max 293 nm, ϵ 2300 M^{-1} cm^{-1}). Concentrations are 9.1 × 10^{-5} M for both tyrosine and tyrosinate solutions.

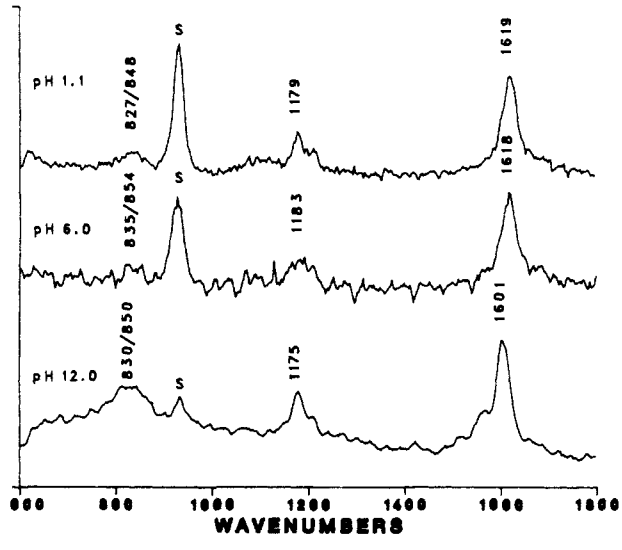

Figure 2. Resonance Raman spectra of fully protonated tyrosine (pH 1.1), zwitterionic tyrosine (pH 6.0), and tyrosinate (pH 12.0) with 230-nm excitation. Incident laser power = 10 mW over a 0.01-cm^2 area in sample capillary. The spectrometer band-pass is 12 cm^{-1}.

electronically forbidden transitions of benzene. While these two transitions in benzene are formally forbidden by symmetry and occur only through vibronic coupling to the E_{1u} ($B_{a,b}$) higher lying excited state, the analogous L_a and L_b transitions in substituted benzene derivatives are not formally forbidden and the decrease in molecular symmetry causes an increase in the oscillator strengths of these transitions.[31,32]

Identical absorption spectra are obtained for fully protonated and zwitterionic tyrosine residues. In contrast, deprotonation of the phenolic hydrogen shifts the L_a absorption maximum from 222 nm in tyrosine to 240 nm in tyrosinate. This shift makes it possible to selectively excite the resonance Raman spectra of tyrosine and tyrosinate in solution, and similarly provides a means by which protonated and deprotonated tyrosyl residues in proteins can be selectively enhanced by UVRR.

Figure 2 shows the 230-nm excited resonance Raman spectra of tyrosine as a function of pH. The spectra shown in Figure 2 were taken with relatively high incident laser powers, so the relative

(30) Asher, S. A. *Appl. Spectrosc.* **1984**, *38*, 276.

(31) Ziegler, L. D.; Hudson, B. S. In *Excited States*; Lim, E. C., Ed.; Academic Press: New York, 1982; Vol. V, p 41.

(32) Platt, J. K.; Klevens, H. B. *Chem. Rev.* **1947**, *41*, 301.

Table I. pH Dependence of the Fundamental Raman Frequencies and Depolarization Ratios of Tyrosine Derivatives

tyrosine[a] pH 1.1	tyrosine[b] pH 6.0	tyrosinate[c] pH 12.0	assignment	
827/848	835/854	830/850 (0.60 ± 0.4)	$2\nu_{16a} + \nu_1$	Fermi resonance involving symmetric ring stretching mode
1179	1183 (0.34 ± 0.11)	1175 (0.39 ± 0.15)	ν_{9a}	in-plane CH bend with a contribution from C_6H_5–C stretching
1210	1209	1208		totally symmetric stretch
1268	1268	1270	ν_{7a}	symmetric ring deformation with ca. 20% contribution from C–O stretch
1603	1601	1556	ν_{8b}	in-plane ring stretching
1619	1618 (0.50 ± 0.03)	1601 (0.37 ± 0.09)	ν_{8a}	in-plane ring stretching

[a] Reference 38. [b] Spectral bandpass used was 12 cm^{-1}. [c] Reference 21.

intensities of tyrosine bands, compared to perchlorate, are artifactually lower (vide infra) than that expected from the relative Raman cross sections of the tyrosine bands. The saturation phenomena observed for tyrosine and tyrosinate, however, do not influence the Raman band frequencies or the relative intensities among tyrosine or tyrosinate bands. Excitation at 230 nm is resonant on the long-wavelength side of the L_a transitions of the fully protonated (pH 1.1) and zwitterionic (pH 6.0) tyrosyl residues, and is resonant on the short wavelength side of the L_a transition maximum of tyrosinate. Deprotonation of the phenolic hydrogen causes frequency shifts of the vibrations. Table I lists the Raman frequencies and the assignments of the vibrational modes of tyrosine (pH 1.1), zwitterionic tyrosine (pH 6.0), and tyrosinate (pH 12.0).[21,23] The vibrational frequencies of tyrosyl residues in proteins may be useful in determining the state of protonation and hydrogen bonding, thereby elucidating the specific local environment of tyrosyl residues.

Excitation in resonance with the L_a $\pi \rightarrow \pi^*$ transition enhances only bands associated with the aromatic side chain of tyrosyl residues. At pH 6.0, zwitterionic tyrosine has a band at 1618 cm^{-1} assigned to the ν_{8a} in-plane ring stretching mode. The peak at 1601 cm^{-1} from the ν_{8b} vibration appears as a shoulder on the 1618-cm^{-1} band with far-UV excitation.[15] The 1183-cm^{-1} band is due to an in-plane CH bending mode that resembles the ν_{9a} mode of benzene. The unresolved doublet at ca. 850 cm^{-1} in both tyrosine and tyrosinate is caused by Fermi resonance between the ν_1 symmetric ring-stretching fundamental and the first overtone of the out-of-plane ν_{16a} ring deformation. A band at 647 cm^{-1} in tyrosine has been assigned to the ν_{6b} ring deformation and is not greatly enhanced in resonance with the L_a transition. The 1268-cm^{-1} C–O stretching vibration is not resonantly enhanced by wavelengths between 250 and 217 nm and is enhanced primarily by transitions further out in the UV.[15,21] Excitation within the L_a transition enhances mostly the 1618- and 1183-cm^{-1} bands. Protonation of the α-amino group results in only slight changes in the vibrational frequencies of the resonantly enhanced modes of the aromatic side chain. Previously reported excitation profiles of tyrosinate in its L_a transition show resonance enhancement of the 830/850 doublet, and the 1175-, 1208-, and 1601-cm^{-1} modes.[21]

Figure 3 shows ultraviolet resonance Raman spectra of tyrosine measured with excitation wavelengths between 217 and 250 nm. The peak at 932 cm^{-1}, due to the symmetric stretching of the perchlorate anion, was numerically removed from each spectrum. Figure 3 qualitatively illustrates the excitation wavelength dependence of enhancement within the L_a absorption band of tyrosine. The spectra were measured with incident energy fluxes of ca. 10 mJ/cm^2·pulse. Thus, the spectral intensities are somewhat influenced by saturation. The peak intensities measured in resonance with the L_a transition in the absence of saturating phenomena would be ca. 40% higher at the peak of the excitation profile than the intensities shown in Figure 3. With excitation at preresonant frequencies, the peak intensities observed depend linearly on the incident power level. Thus, the true relative enhancement maximum at ca. 225 nm is actually more dramatic than that apparent from Figure 3.

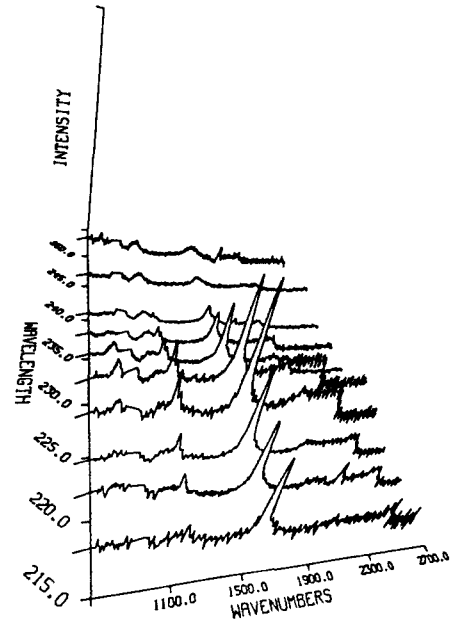

Figure 3. The ultraviolet resonance Raman spectra of tyrosine between 217 and 250 nm. The spectra have been scaled such that the intensity of the sodium perchlorate internal standard is constant. The internal standard peak was then numerically subtracted from each spectrum.

Figure 4 shows the dependence of the measured Raman intensity on the incident laser power with 230-nm excitation. Figure 4A shows the Raman intensity of the tyrosine and the internal standard perchlorate bands as a function of incident laser power. As expected, the Raman intensity of the perchlorate band increases linearly with laser power. The Raman intensities of the tyrosine bands, however, increase linearly only at the lowest incident laser powers. Saturation is particularly evident for the Fermi resonance doublet at ca. 850 and the 1183-cm^{-1} band. Saturation is less evident for the 1618-cm^{-1} band since part of its intensity derives from the ca. 1650-cm^{-1} water O–H bending vibration which does not saturate.

Figure 4B gives clearer insight into the saturation of the Raman bands. Saturation is clearly evident for all bands when relative intensities of tyrosine to perchlorate are plotted. For incident energy fluxes below 1 mJ/cm^2·pulse (1 mW average laser power) the relative ratios are close to that found by extrapolation to zero laser energy flux, indicating that little saturation is present. At higher fluxes, however, the relative ratios decrease, indicating the suppression of tyrosine bands by saturation. Thus, the absolute Raman cross section of tyrosine must be measured with incident energy fluxes below 1 mJ/cm^2·pulse and extrapolated to zero energy flux.

The absorption spectrum and the total differential Raman cross-section excitation profiles of the 1183- and 1618-cm^{-1} bands and the 835/854-cm^{-1} doublet of tyrosine measured at low incident power densities are shown in Figure 5. The Raman cross sections increase dramatically as the excitation frequency approaches the L_a absorption maximum. The excitation profile maxima at 225 nm occur on the long-wavelength side of the apparent absorption maximum at 222 nm. For both tyrosinate and tyrosine, the ν_{8a} band at ca. 1600 cm^{-1} dominates the Raman spectra excited within the L_a transition. The ν_{8b} mode is also resonantly enhanced within the L_a transition,[15] but was not resolved from the ν_{8a} band in our

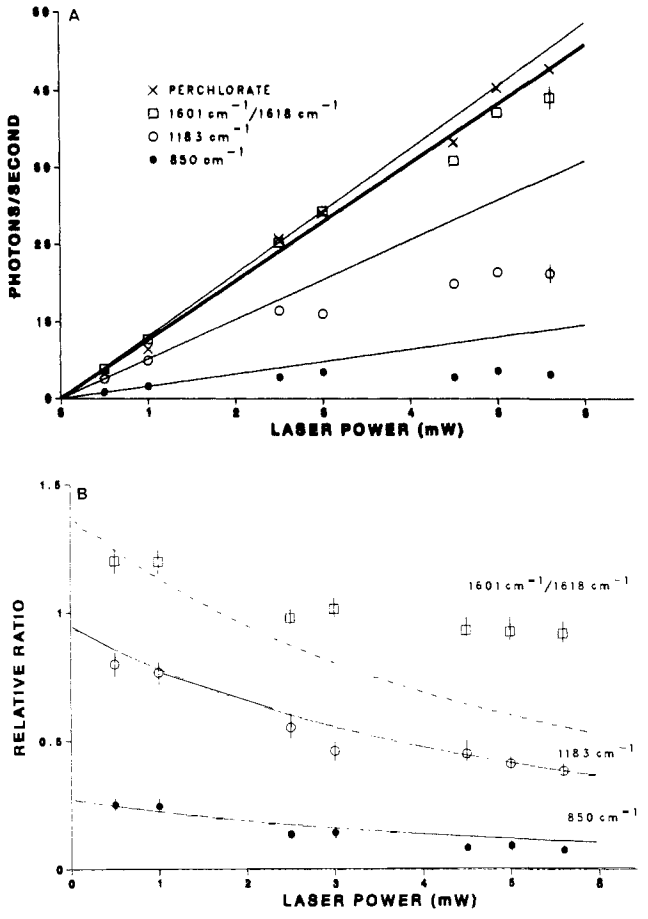

Figure 4. Laser power dependence of tyrosine Raman scattering (2 mM, pH 6.0). The spectra were taken with 230-nm excitation and the beam was focused to a 0.1-cm diameter on the sample. Neutral density filters were used to attenuate the incident power. (A) Absolute Raman intensity dependence. The lines plot the Raman intensity in the absence of saturation. The thick line shows the observed perchlorate intensity. (B) Relative Raman intensity dependence of the tyrosine peak relative to the perchlorate peak. The lines were calculated from eq 8. The measured Raman intensity for the 1601/1618-cm^{-1} peak (dashed curve) has not been corrected for water interference. The perchlorate concentration was 1.0 M.

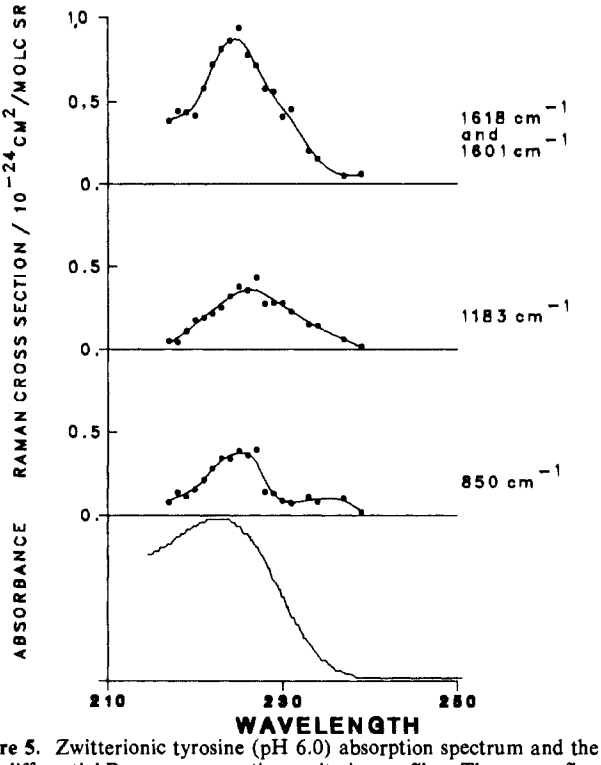

Figure 5. Zwitterionic tyrosine (pH 6.0) absorption spectrum and the total differential Raman cross-section excitation profiles. The energy flux within the sample was less than 1 mJ/cm^2·pulse. The estimated relative standard deviation of the measured values is ca. 10%. The lines were drawn to help visualization of the band shape of the Raman excitation profiles.

low-resolution excitation profile data. The ν_{8a} band of tyrosinate is maximally enhanced with 245-nm excitation with an absolute Raman cross section of 0.53 barn/sr (barn (b) = 10^{-24} cm^2/mol), while the ν_{8a}, ν_{8b} band of the zwitterion is maximally enhanced at 225 nm with an absolute Raman cross section of 1.0 barn/sr. The ν_{7a} mode shows little enhancement in resonance with the L_a transition for both tyrosine and tyrosinate. The ν_{9a} and Fermi resonance doublet bands of tyrosine, at 1183 and ca. 850 cm^{-1}, respectively, show cross sections of ca. 0.4 b/sr. The excitation profiles of the enhanced modes of tyrosine are considerably narrower than the corresponding excitation profiles of tyrosinate. The excitation profile full width at half-maximum for tyrosine is ca. 2000 cm^{-1} (10 nm) for the 1618-cm^{-1} mode as compared to ca. 3700 cm^{-1} (20 nm) for tyrosinate.

Figure 6 shows the effect of saturation on the measured Raman excitation profiles. Figure 6A shows the absorption spectra of tyrosine along with the excitation profile of the 1618/1601-cm^{-1} band previously displayed in Figure 5, as well as the excitation profile measured under saturating conditions. The excitation profiles are almost identical at longer wavelengths; however, saturation becomes evident in a decrease in cross section as excitation occurs at shorter wavelengths, as, for example, at 230 nm with energy fluxes of 10 mJ/cm^2·pulse. Saturation is most pronounced with excitation at the absorption band maximum. Figure 6B similarly shows the effects of saturation on the 1183-cm^{-1} band excitation profile. In both cases, the apparent Raman cross section at the excitation profile maximum under saturating conditions is ca. 60% of that for the unsaturated band. The excitation profiles measured under saturating conditions qualitatively follow the shape of the unsaturated excitation profiles.

The depolarization ratios of the 1618- and 1183-cm^{-1} bands are listed in Table I. The depolarization ratio of the 1183-cm^{-1} band is ca. 0.34, indicating an *A*-term scattering mechanism where a single diagonal element of the polarizability tensor dominates. The depolarization ratio of the 1618-cm^{-1} band was measured as 0.50. This band, however, is not resolved from the 1611-cm^{-1} ν_{8b} band with the slit settings necessary to measure the depolarization ratio. The laser intensities used for the depolarization ratio measurements were above threshold for saturation. This will not affect the measured values, however, because only the ground-state tyrosines contribute to the Raman scattering (vide infra).

Discussion

The L_a transitions of tyrosine and tyrosinate derive from the B_{1u} transition of benzene. The B_{1u} transition is formally forbidden in benzene, but has a nonzero oscillator strength because of Herzberg–Teller coupling to the allowed E_{1u} state by vibrations of e_{2g} symmetry. In the C_{2v} point group of para-substituted benzene derivatives, the B_{1u} excited state transition assumes A_1 symmetry. The transition, now designated as L_a, is no longer symmetry forbidden because of the decrease in symmetry from D_{6h} to C_{2v}. Vibrational modes with atomic displacements along bonds which undergo bond length and electron density changes between the ground and the L_a excited state will be resonantly enhanced by excitation within the L_a transition. The degeneracy of the e_{2g} vibrational modes of benzene will be lifted by the decrease in symmetry, and modes of a_1 and b_1 symmetry will appear. The a_1 modes can be enhanced by the Franck-Condon *A*-term mechanism.[21,34,37]

The vibrational modes enhanced in resonance within the L_a absorption bands are identical in tyrosine and tyrosinate (Table I).[21,33,34] The enhanced vibrations derive solely from in-plane

(33) Baron, M. H.; Loze, C.; Mejean, T.; Coulange, M. J. *J. Chem. Phys.* **1983**, *80*, 729.

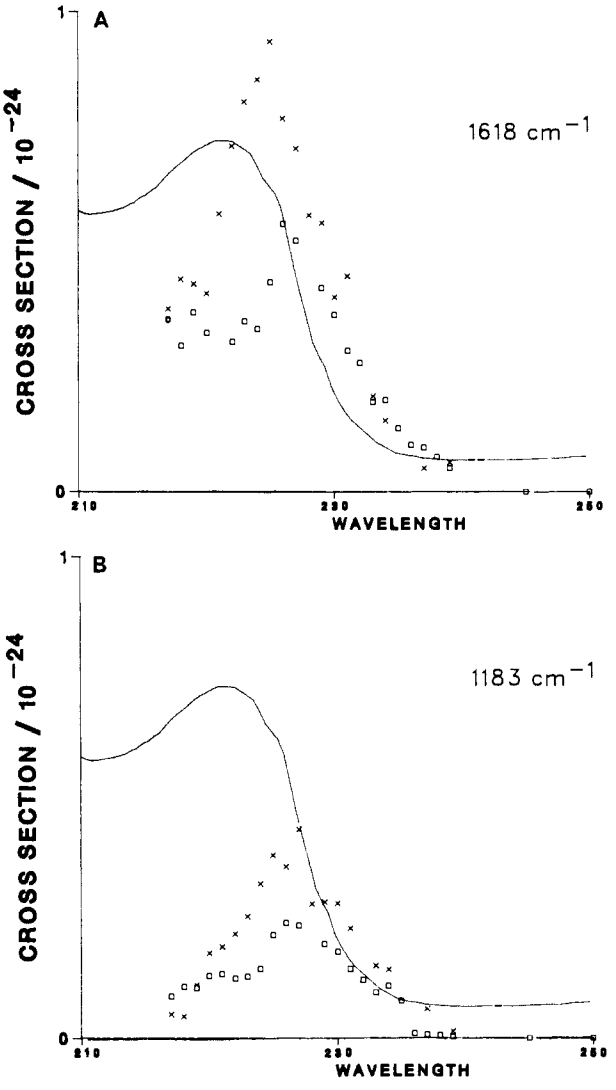

Figure 6. (A) Zwitterionic tyrosine (pH 6.0) absorption spectrum and the total differential Raman cross-section excitation profile of the 1601/1618-cm^{-1} tyrosinate band measured with energy densities within the sample of less than 1 mJ/cm^2·pulse (×) and 10 mJ/cm^2·pulse (□). (B) Zwitterionic tyrosine (pH 6.0) absorption spectrum and the total differential Raman cross-section excitation profile of the 1183-cm^{-1} band measured with energy densities within the sample of less than 1 mJ/cm^2·pulse (×) and ~10 mJ/cm^2·pulse (□). The cross-section units are cm^2/mol·sr.

vibrations of the aromatic rings. The ν_1 vibration is enhanced as part of the Fermi resonance doublet at 830/850 cm^{-1}. Strongly enhanced modes deriving from the ν_{8a} and ν_{9a} vibrations of benzene occur at 1618 (1601 cm^{-1}) and 1183 (1175 cm^{-1}) in tyrosine (tyrosinate). The totally symmetric stretching mode of para-substituted benzene derivatives occurs at ca. 1210 cm^{-1} in both tyrosine and tyrosinate. The 1270-cm^{-1} peak derives from a vibration with a large contribution from the C–O stretch.[35]

The ν_{8b} band of tyrosine at 1601 cm^{-1} is not resolved from the ν_{8a} band, but is enhanced within the L_a transition.[15] The ν_{7a} mode at 1270 cm^{-1} is not enhanced for tyrosine or tyrosinate within the L_a transition.[15,21] The excitation profile data for the 835/854-cm^{-1} Fermi resonance doublet represents the total intensity for both peaks in the doublet. The spectral resolution used was too low to determine the individual intensities; however, the band shapes observed with excitation throughout the L_a transition suggest that no large changes occur in the relative intensity. The same result occurs for the excitation profile of the 830/850-cm^{-1} band of tyrosinate, indicating that similar excitation profiles occur for both components of the doublet in tyrosine and tyrosinate. This is an important observation because the relative intensity of this doublet has been used in nonresonance Raman studies to monitor the degree of hydrogen bonding of the phenolic hydroxyls of tyrosyl residues in proteins.

Table II. Total Differential Raman Cross Sections[a] of Tyrosine and Tyrosinate

Raman band, cm^{-1}	excitation wavelength				
	220	225	230	240	250
		Tyrosine			
835/854	0.15	0.38	0.08	0.02	
1183	0.18	0.38	0.28	0.015	
1601/1618	0.41	0.94	0.41	0.061	
		Tyrosinate			
830/850	0.05		0.078	0.10	0.07
1175	0.075		0.10	0.18	0.17
1601	0.22		0.21	0.40	0.28

[a] Cross section units are barns/sr (10^{-24} cm^2/mol·sr). The tryosinate cross sections in this table were remeasured using lower energy fluxes than those used in ref 21. The cross sections were determined by extrapolation to zero energy flux as described in ref 39.

Table III. UV Absorption Spectral Data for Tyrosine and Tyrosinate[a]

	λ_{max}	ϵ, M^{-1} cm^{-1}	λ_{max}	ϵ, M^{-1} cm^{-1}	λ_{max}	ϵ, M^{-1} cm^{-1}
tyrosine	275	1400	222	9000	193	36000
tyrosinate	293	2300	240	11000	*b*	

[a] Reference 37. [b] Overlaps with OH^- absorption.

The Raman cross sections for the enhanced peaks of tyrosinate and tyrosine are listed in Table II. Deprotonation of the phenolic hydrogen of tyrosine moves the L_a absorption band from an apparent maximum of 222 nm in tyrosine to 240 nm in tyrosinate.[36] Consequently, maximal enhancement occurs at longer wavelengths for tyrosinate (245 nm) than tyrosine (225 nm). Table III lists the UV absorption spectral data for tyrosine and tyrosinate. The choice of excitation wavelengths for the study of particular tyrosyl residues in proteins may be guided by the excitation profiles of tyrosine presented here, and our previously reported tyrosinate excitation profiles.[21]

The UV absorption spectrum of tyrosine shows that the L_a transition overlaps the higher energy $B_{a,b}$ transition. Consequently, the true absorption maximum of the L_a transition is somewhat red-shifted from the apparent maximum. Indeed, each of the excitation profiles shown in Figure 5 are probably red-shifted from the observed absorption maximum because they follow the true absorption spectrum. We do not believe this red shift derives from destructive interference phenomena because the excitation profiles are symmetric about their maxima. The excitation profiles of tyrosine are not as structured as that of tyrosinate. The larger bandwidth and more Gaussian band shape of the tyrosinate excitation profiles suggest that the excitation profiles of tyrosinate are more inhomogeneously broadened than tyrosine, which would be consistent with the expected larger tyrosinate–solvent interactions. Strong hydrogen bonding to the deprotonated phenolic oxygen will occur. The more Lorentzian excitation profiles of tyrosine suggest less inhomogeneous broadening. The single excitation profile maximum at 225 nm may indicate comparable enhancement for the 0–0 and 0–1 transitions. This contrasts with the partially resolved 0–0 and 0–1 excitation profile maxima observed earlier for tyrosinate.

Excitation within the L_a transition results in strong enhancements of a_1 symmetry vibrational modes. The maximum total differential Raman cross-section value for tyrosine is 0.94 b/sr for the ν_{8a}, ν_{8b} band with 225-nm excitation. In contrast, the

(34) Albrecht, A. C. *J. Chem. Phys.* **1961**, *34*, 1476.
(35) Wilson, E. B., Jr. *Phys. Rev.* **1934**, *45*, 706.
(36) Grinspan, H.; Birnbaum, J.; Feitelson, J. *Biochim. Biophys. Acta* **1966**, *126*, 13.
(37) Edelhoch, H. *Biochemistry* **1967**, *6*, 1948.
(38) (a) Pigeon Gusselin, M.; Pezulet, M., unpublished results. (b) Baron, M. H.; deLuze, C.; Mejean, T.; Curlange, M. J.; Turpin, P. Y.; Chinsky, L. *J. Chim. Phys.* **1983**, *80*, 729.

maximum value for the total differential Raman cross section of the tyrosinate ν_{8a} mode at 245 nm is 0.53 b/sr.[21] This difference may be related to the differences in the homogeneous and inhomogeneous broadening present in the absorption spectra. The bandwidth of the excitation profile of the ν_{8a}, ν_{8b} band of tyrosine is half that for tyrosinate: ca. 10 nm (2000 cm^{-1}) compared to ca. 20 nm (3700 cm^{-1}). If inhomogeneous broadening dominates, the maximum Raman cross section will be inversely proportional to the bandwidth. A higher cross-section dependence on bandwidth (which is complex) is expected if homogeneous broadening dominates the absorption vibronic envelope. Thus, the difference in cross sections is related to the absorption bandwidth. We are presently examining this dependence in detail.

Attempts to measure the total differential Raman cross sections of tryptophan and pyrene with our present pulsed laser source were unsuccessful because of the large saturation which occur for these molecules.[21,29] The excitation profiles shown in Figure 6 demonstrate that saturation alters the measured excitation profiles, especially as the excitation frequency approaches the absorption band maximum. In the case of tyrosine, the excitation profile maximum position is not dramatically shifted by saturation provided the power density used is kept constant. However, high laser excitation power densities cause a decrease in the measured total differential Raman cross sections which result in an artifactual broadening of the measured excitation profile.

Saturation may result from a decrease in the number of ground-state molecules during the laser pulse. The decrease in Raman intensity due to saturation occurs through a simple mechanism whereby the incident photon produces either Raman scattering (I_p) or removes ground-state molecules (P) from the sampling volume:[28]

$$I_p \xleftarrow[\sigma_p]{} P \xrightarrow[\sigma_a]{} S \tag{1}$$

where σ_p is the cross section for Raman scattering at the excitation frequency ν, and S is the bottleneck state responsible for the depletion of the ground state. In tyrosine, high power densities may convert a significant population of molecules to the first singlet excited state, or to a transient radical cation species similar to that reported for tyrosinate.[28] In either case, the Raman scattering from these new species is apparently not strongly enhanced by excitation within the L_a transition of ground-state tyrosine. Once a molecule is removed from the ground state, it cannot contribute to Raman scattering until it decays back into the ground state.

The laser pulse intensity at time t can be described as:

$$I(t) = I_0 L(t) \tag{2}$$

where I_0 is the total energy/cm^2 of the pulse (integrated over time) and $L(t)$ is the normalized temporal band shape function of the pulse. The rate of disappearance of ground-state molecules is modeled:

$$-dP/dt = \sigma_a I(t) P_0 \tag{3}$$

where σ_a is the product of the absorption cross section and the probability of reaching the bottleneck state or states. The concentration of ground-state molecules at time t during the pulse is therefore:

$$P(t) = P_0 e^{-\sigma_s I_0 \int_0^t L(t)\,dt} \tag{4}$$

where P_0 is the initial concentration of P. The Raman intensity at frequency ν from a given constant volume of tyrosine integrated over the time of the laser pulse is:

$$I_p(\nu) = \sigma_p I_0 P_0 \int_0^\infty L(t) e^{-\sigma_s I_0 \int_0^t L(t)\,dt} \tag{5}$$

After integration the observed Raman intensity is

$$I_p(\nu) = (\sigma_p P_0/\sigma_a)(1 - e^{-\sigma_s I_0}) \tag{6}$$

The Raman intensity of the nonabsorbing internal standard is

$$I_s(\nu) = \sigma_s I_0 C_0 \tag{7}$$

where σ_s and C_0 are the scattering cross section at the excitation frequency and the concentration of the internal standard, respectively. The relative ratio of the tyrosine peak to the internal standard peak as a function of incident laser power is:

$$R(\nu) = \frac{\sigma_p P_0}{\sigma_a \sigma_s I_0 C_0}(1 - e^{-\sigma_s I_0}) \tag{8}$$

Assuming that a molecule which absorbs a photon does not relax back to the ground state during the 4-ns laser excitation pulse, σ_a is identical with the absorption cross section and is proportional to the molar absorptivity $\epsilon(\nu)$. Equation 8 indicates that the degree of saturation is independent of analyte concentration within the approximation that the intensity of excitation is uniform throughout the sampling volume. For highly concentrated, high optical density solutions, a concentration dependence for saturation may be observed. This behavior can only be modeled if the sampling volume is carefully defined.

We can use $R(\nu)$ from eq 8 to calculate the effect of saturation on Raman excitation profiles as shown by Figure 4B. Figure 7 shows the effect of increasing laser power on the excitation profile of tyrosine. The L_a absorption spectrum of tyrosine is closely simulated with a Lorentzian band shape of ca. 14-nm bandwidth with a maximum molar absorptivity of 9000 M^{-1} cm^{-1}. We model two cases where the Raman excitation profile is shifted relative to the absorption (Figure 7A, absorption λ_{max} 222 nm), and where the excitation profile maximum is coincident with the absorption (Figure 7B, absorption λ_{max} 225 nm). Equation 8, which intrinsically assumes that the population of the bottleneck state is directly proportional to molar absorptivity, predicts that increasing the incident laser power will suppress the relative ratio of ground-state tyrosine molecules to internal standard molecules. This will result in a decrease and a broadening of the measured excitation profile. The model also predicts that if the excitation profile maximum is not coincident with the absorption maximum, the excitation profile will be skewed and differentially attenuated on the high absorption side. The experimental excitation profiles of the tyrosine 1618- and 1183-cm^{-1} bands in Figure 6, A and B, measured under both saturating and nonsaturating conditions, show that the saturated excitation profile maximum may be slightly shifted to longer wavelength, away from the absorption band maximum.

Laser excitation in the UV with pulsed sources may produce detectable photochemical species or saturation at high power densities. The UVRR spectrum of tyrosinate at high power densities shows bands at 1402, 1510, and 1565 cm^{-1} assigned to tyrosyl radical.[28] Peaks attributable to this species also appear in the UVRR Raman spectrum of tyrosine at high power densities; the pK_a of tyrosyl radical cation is less than 1.0. Tyrosine photochemical intermediates are harder to detect than that of tyrosinate either because of smaller cross sections for production, or because they have smaller Raman cross sections.

The results presented here indicate that tyrosine and tyrosinate groups can be selectively studied in proteins. The maximum enhancements for both tyrosine and tyrosinate occur in the UV within their 220- and 250-nm L_a absorption bands. The upper panel of Figure 8 shows the selectivity available for enhancement of these residues in a plot of the log of the ratio of tyrosine to tyrosinate Raman cross sections. The lower panel indicates the sensitivity by plotting the average Raman cross section. This comparison between the tyrosine and tyrosinate cross sections combined with that of other residues can be utilized to determine the selectivity available for aromatic amino acid residues within a particular protein. For example, the cross section of tyrosinates is ca. ten times that of tyrosine at 245-nm excitation while the average cross section is about 50% of the maximum value; the tyrosine cross section is low. Excitation at 245 nm can be used to observe the formation of tyrosinate, while 225-nm excitation examines tyrosine residues. This plot for tyrosine and tyrosinate is only a guideline for protein studies since the magnitude of the tyrosyl cross sections, the excitation profile widths, and the Raman frequencies will depend upon the environment and hydrogen bonding of these residues.

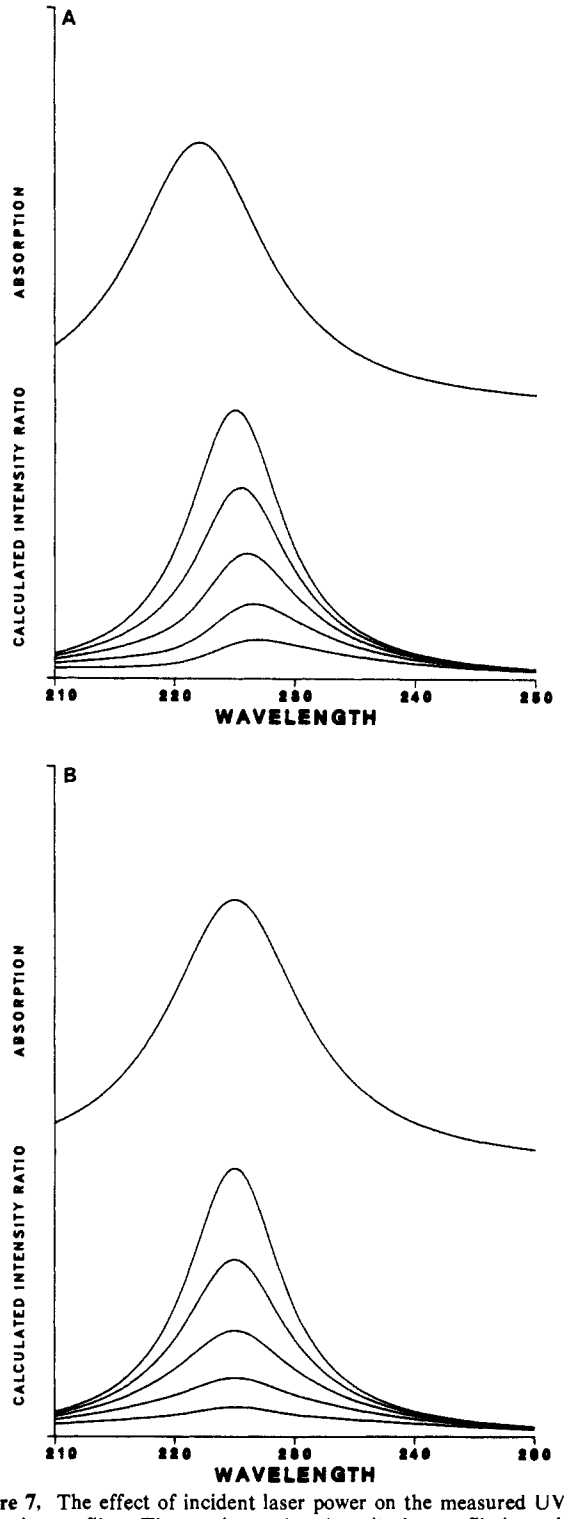

Figure 7. The effect of incident laser power on the measured UVRR excitation profiles. The maximum (true) excitation profile is modeled as a Lorentzian with a bandwidth of ca. 10 nm. The lower excitation profiles were calculated using incident laser powers of 1, 2.5, 5.0, and 10 units, respectively. The absorption spectrum was simulated by using a Lorentzian line shape with a ca. 14-nm bandwidth and a molar absorptivity of 9000 M^{-1} cm^{-1}. (A) Effect of increase in laser power on an excitation profile which is shifted with respect to the absorption band. (B) Effect of increase in laser power on an excitation profile whose maximum is coincident with that of the absorption band.

The saturation phenomena observed are indeed impediments for Raman spectral measurements in proteins. The susceptibility for saturation is a function of the relaxation rate of the residue, the excitation wavelength, and the effective power density at that residue in the protein (i.e., internal filtering may be important). Thus, with the typical excitation source we may expect changes

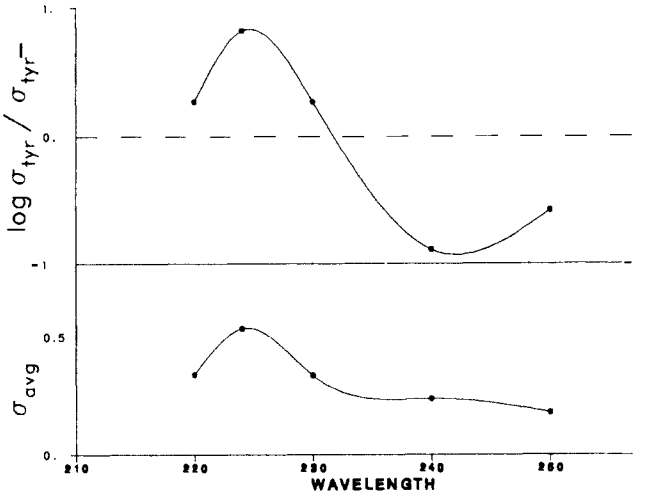

Figure 8. Selectivity plot for Raman enhancement for tyrosine and tyrosinate. The values of the cross-section ratios are derived from data of Figure 5 and Asher et al.[21] and remeasured data for tyrosinate obtained with either a high-repetition-rate excimer-based UV laser source or by extrapolating the YAG excitation data to zero incident energy flux.[39] The units for the average Raman cross section for tyrosine and tyrosinate are barns/sr (10^{-24} cm^2/mol·sr).

in relative intensities due to small alterations in solution and experimental conditions as the relative saturation of different residues change. Not only will this lead to changes in relative intensities but also frequency shifts can be observed for overlapping bands where the degree of saturation of one component differs from another. We have already demonstrated the complexity which is possible if the bottleneck state, such as the tyrosyl radical, is resonance enhanced and new bands appear.[28]

The solution to these difficulties is a lower peak power UV excitation source. We are presently constructing one centered around a high repetition rate excimer laser.[39] However, the saturation phenomena themselves are of interest since they are related to the relaxation rates of residues. For example, if the bottleneck is a singlet state in a heme protein, Förster transfer would result in residues near the heme being less susceptible to saturation than those further away. The relaxation behavior of residues will be exquisitely sensitive to environment and "saturation Raman spectroscopy (SRS)" may become an important new technique in itself.

Conclusion

The total differential Raman excitation profile cross sections of tyrosine have been measured between 217 and 240 nm in the L_a absorption of tyrosine. Vibrational modes of a_1 symmetry with atomic displacements along bonds which undergo changes in bond length and electron density upon excitation to the L_a excited state are resonance enhanced by the Franck-Condon *A*-term mechanism. The cross sections of tyrosine presented here and the previously reported cross sections of tyrosinate can be used for determining the selectivity available for the study of tyrosyl residues in proteins as a function of excitation wavelength.[21] The excitation profiles of tyrosine were measured with low incident laser powers to avoid saturation phenomena. A model is developed for optical saturation which predicts the effect of increasing laser power densities on Raman spectral measurements.

Acknowledgment. We gratefully acknowledge support of this work from NIH Grant 1R01 GM30741-06. Sanford A. Asher is an Established Investigator of the American Heart Association; this work was done during the tenure of an Established Investigatorship of the American Heart Association, Pennsylvania affiliate.

Registry No. Tyrosine, 60-18-4.

(39) Jones, C. J.; DeVito, V. L.; Harmon, P. A.; Asher, S. A. *Appl. Spectrosc.* **1987**, *41*, 1268.